Received: 31 March 2026 | Revised: 3 June 2026 | Accepted: 17 July 2026 | Published online: 11 August 2026

Journal of Optics and Photonics Research
2026, Vol. 00(00) 1–14
DOI: 10.47852/bonviewJOPR62029745

REVIEW

Recent Advances in Polarization Control for Fiber Links: Mechanisms, Technologies, and Applications

Zhihang Zhang[1], Yujie Zheng[1], Xiao Wu[1], Jianhua Yang[1], Heming Wei[2,*], Long Ma[3], Xiaohu Liu[4], Dapeng Han[5], Lijun Miao[5,*] and Dengwei Zhang[1]

[1] *State Key Laboratory of Extreme Photonics and Instrumentation, Zhejiang University, China*

[2] *The Key Laboratory of Specialty Fiber Optics and Optical Access Networks, Shanghai University, China*

[3] *Nantong Jichangbao Technology Co., Ltd, China*

[4] *National Key Laboratory of Test & Evaluation of ElectroMagnetic Space Security, China*

[5] *Advanced Technology Institute, Zhejiang University, China*

Abstract: Polarization control is essential for maintaining the performance and stability of fiber-optic sensing and optical communication systems, since the state of polarization in fiber links is highly susceptible to birefringence variation and environmental perturbations. This review summarizes recent advances in polarization control for fiber links from the perspectives of polarization-evolution mechanisms, target performance parameters, application-specific requirements, and representative technical implementations. Passive polarization-control schemes are first discussed, with emphasis on loop-based architectures, all-polarization-maintaining configurations, and integrated passive approaches. Active polarization-control techniques are then reviewed, including manual fiber polarization controllers, Faraday-effect-based devices, lithium-niobate electro-optic controllers, and other emerging platforms such as silicon photonics and liquid-crystal-integrated devices. Their operating principles, structural characteristics, and key performance metrics are compared. Recent progress shows that the field is evolving from static and discrete schemes toward high-speed, closed-loop, and highly integrated architectures. Despite these advances, achieving a balanced combination of low loss, high extinction ratio, ultrafast response, low power consumption, compact footprint, and long-term stability remains a major challenge for practical deployment.

Keywords: fiber polarization control, polarization-maintaining fiber, integrated photonics

1. Introduction

Fiber-optic sensing and optical communication have become key technologies for modern information transmission and intelligent sensing due to their high bandwidth, low loss, and strong immunity to electromagnetic interference [1–3]. Stable transmission and precise control of the state of polarization in optical fibers are crucial for enhancing the performance of fiber-optic sensing and optical communication systems [4]. However, the state of polarization in fiber links is easily disturbed by temperature variations, mechanical vibration, bending, twisting, and external stress. Such perturbations may induce random polarization drift, resulting in polarization-dependent loss, polarization crosstalk, and deterioration of system stability [5, 6]. According to their technical routes, polarization control in fiber links can be broadly classified into passive polarization control and active polarization control. Passive polarization control mainly relies on fixed birefringent components, polarization-selective devices, or specially designed fiber structures to control the state of polarization without real-time external regulation [7]. Active polarization control operates by introducing externally driven electric, magnetic, or stress fields to dynamically modify the phase relationship or coupling between orthogonal polarization components, thereby enabling real-time regulation of the state of polarization. According to the implementation platform, active polarization control can be generally classified into fiber-based discrete devices [8], bulk-optic devices [9], and integrated photonic devices [10]. Compared with passive polarization control, active polarization control offers higher control accuracy, faster response speed, and stronger adaptability to dynamic polarization fluctuations but usually involves greater system complexity, higher power consumption, and more demanding control strategies [11].

***Corresponding authors:** Heming Wei, The Key Laboratory of Specialty Fiber Optics and Optical Access Networks, Shanghai University, China. Email: hmwei@shu.edu.cn and Lijun Miao, Advanced Technology Institute, Zhejiang University, China. Email: mlj000000@zju.edu.cn

Nevertheless, current research is still constrained by the difficulty of simultaneously reducing locking time, suppressing polarization fluctuation, and maintaining a compact and low-power system architecture, which remains a key challenge for practical fiber-link polarization control.

The rapid development of fiber-optic sensing and coherent optical communication technologies has promoted extensive research on polarization control in fiber links. Existing review articles have provided valuable discussions on specific polarization-control devices, modulation mechanisms, or application scenarios, offering important references for the development of related technologies [12]. However, most current reviews mainly focus on individual technical routes or isolated application systems, while comparatively limited attention has been given to the systematic relationships among polarization-evolution mechanisms, application-oriented requirements, target performance parameters, and representative implementation strategies [13].

By reviewing the recent advances in polarization-control technologies for fiber links, this paper aims to provide a valuable reference for researchers and engineers in this field. It first introduces the mechanisms of polarization evolution and the corresponding requirements for polarization control in fiber links, followed by a review of representative passive and active polarization-control technologies from the perspectives of operating principles, structural characteristics, and performance metrics. Finally, the current challenges and future development trends of polarization control for fiber links are discussed to further promote their applications in fiber-optic sensing, optical communication, and related photonic systems.

2. Polarization Evolution and Polarization-Control Requirements in Fiber Links

2.1. Mechanisms of polarization evolution in optical fibers

An ideal single-mode fiber supports a pair of degenerate orthogonal polarization eigenmodes. In practical fiber links, however, this ideal degeneracy is broken by fiber-core geometric asymmetry, residual stress, external loading, and environmental perturbations, which introduce birefringence and cause the two orthogonal polarization modes to exhibit different propagation constants and phase delays [14]. Intrinsic birefringence mainly originates from core ellipticity and residual stress introduced during fabrication, whereas bending, twisting, stretching, and temperature variations further modify the local refractive-index distribution during propagation and thereby induce additional birefringence [15]. For example, bending can generate birefringence through the combined effects of transverse stress and waveguide deformation, whereas twisting changes the orientation of local polarization eigenaxes and leads to twist-related birefringence [16]. Temperature variations can also alter birefringence through both thermo-optic and thermally induced stress effects [17, 18].

To investigate the effects of stretching and temperature variation on the birefringence of polarization-maintaining (PM) fiber, a two-dimensional cross-sectional finite-element model was established in COMSOL Multiphysics. The stress distribution under different perturbation conditions was first calculated through coupled solid-mechanics and heat-transfer simulations, and the resulting refractive-index variation was then used to evaluate the changes in effective modal index and birefringence. The geometric parameters were set as follows: core radius, 5 μm; cladding radius, 62.5 μm; stress-rod radius, 20 μm; and stress-rod spacing, 32.5 μm. The operating wavelength was 1.55 μm, corresponding to a frequency of 1.934×10^{14} Hz. The initial refractive indices of the core, cladding, and stress region were 1.456, 1.444, and 1.442, respectively. The photoelastic coefficients were A = 0.7572×10^{-12} m^2/N, B = 4.1878×10^{-12} m^2/N, and C = 3.4306×10^{-12} m^2/N. The density, Poisson's ratio, and Young's modulus were 2200 kg/m^3, 0.17, and 78 GPa, respectively. The thermal expansion coefficients of the core, cladding, and stress region were 1.06×10^{-6} K^{-1}, 0.54×10^{-6} K^{-1}, and 2.15×10^{-6} K^{-1}, respectively. The model was discretized with triangular elements and locally refined in the core and its surrounding region. The stretching condition was simulated by applying a 300 N boundary load to the outer cladding boundary, whereas the temperature condition was imposed in the heat-transfer module using an out-of-plane heat flux at 298.5 K with thermal insulation applied to the outer boundary. For the temperature condition, the applied thermal load first generated a nonuniform thermal-stress distribution because of the mismatch in thermal expansion coefficients among different regions, and the resulting stress-optic refractive-index variation was then used to evaluate the birefringence change.

As shown in Figure 1(a)–(c), under stretching, the two orthogonal polarization eigenmodes remained mainly confined within the fiber core, but their effective modal indices showed clear splitting. The effective refractive indices of mode 1 and mode 2 were approximately 1.4539 and 1.4533, respectively, corresponding to a difference of about 6.0×10^{-4}, indicating a pronounced enhancement of modal birefringence. The electric-field distributions show that both modes remained highly localized in the core, with a peak field magnitude on the order of $2.8 \times 10\hat{2}$ V/m, while their principal polarization orientations were aligned along the horizontal and vertical directions, respectively. The stress distribution further reveals a strongly nonuniform field across the fiber cross-section, with significant stress concentration near the outer edges of the two stress regions. The maximum von Mises stress reached approximately 3.7×10^8 N/m^2, whereas the stress near the core was on the order of 10^8 N/m^2. These results indicate that tensile loading enhances birefringence by modifying the transverse stress field and the corresponding refractive-index tensor, thereby increasing the separation between the effective indices of the two orthogonal polarization modes. Figure 1 (d)–(f) shows the simulation results of the effect of temperature variation on the birefringence of the PM fiber. The two orthogonal polarization eigenmodes remained mainly confined within the core, and both electric-field plots exhibited effective modal indices of approximately 1.453, indicating only a small index splitting under the applied thermal condition. The peak electric-field magnitude remained on the order of 2.8×10^2 V/m, and the two eigenmodes preserved their horizontal and vertical polarization orientations, suggesting that the temperature perturbation did not alter the fundamental orthogonal modal characteristics of the PM fiber. The third plot, although labeled as a temperature-related result, actually shows the thermally induced von Mises stress distribution rather than the temperature field itself. A clear thermal-stress concentration appeared near the outer edges of the two stress regions, with a maximum value of approximately 4.7×10^5 N/m^2, while the stress near the core remained relatively low, on the order of 10^5 N/m^2. Overall, the applied temperature variation mainly affected the birefringence through nonuniform thermal stress and the associated refractive-index perturbation, but its influence on stress magnitude and modal index splitting was weaker than that of the stretching condition.

Figure 1

Birefringence simulation of a panda-type polarization-maintaining fiber under stretching and temperature variation: (a) stress distribution in a panda-type polarization-maintaining fiber under stretching, (b) electric-field distribution of the x-polarized eigenmodes under stretching, (c) electric-field distribution of the y-polarized eigenmodes under stretching, (d) stress distribution in panda-type polarization-maintaining fiber under temperature variation, (e) electric-field distribution of the x-polarized eigenmodes under temperature variation, and (f) electric-field distribution of the y-polarized eigenmodes under temperature variation

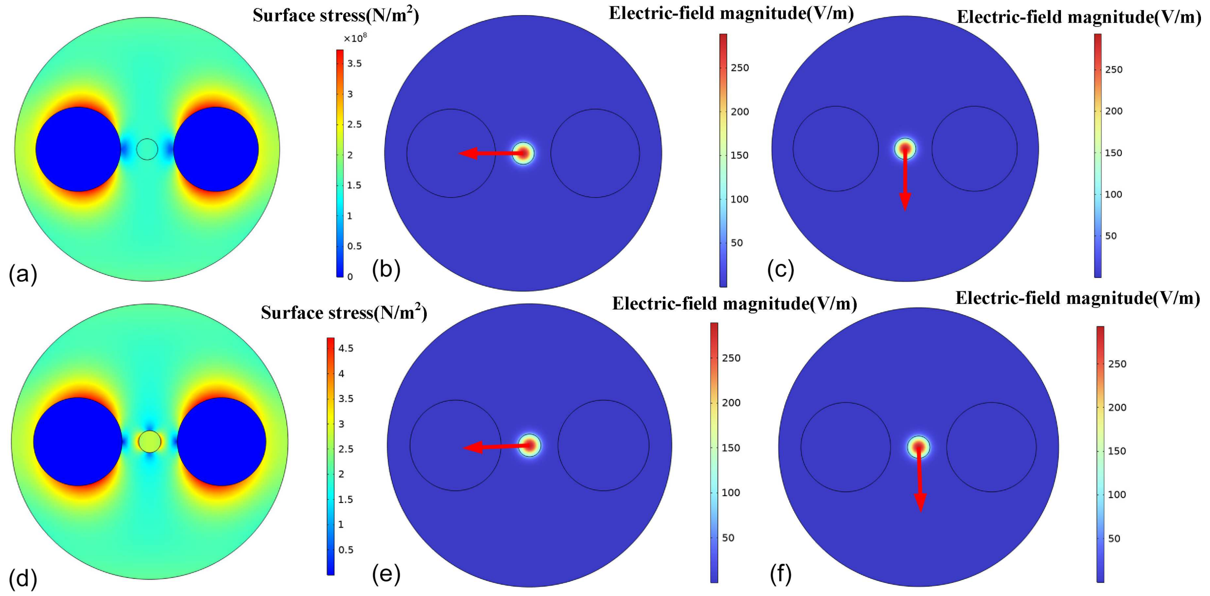

Because birefringence in practical fiber links usually varies randomly along the fiber length, the state of polarization does not remain constant during propagation but instead exhibits polarization-mode coupling and stochastic polarization evolution. When the direction and magnitude of local birefringence vary with position or time, the input polarization components are continuously projected onto and redistributed among different eigenstates, causing the output polarization state to drift along complicated trajectories on the Poincaré sphere. In long-haul links or in environments with strong perturbations, this random evolution may further manifest as polarization-mode dispersion, polarization-state fluctuation, and unstable transmission behavior [19]. From a system perspective, stochastic polarization evolution is the fundamental reason why polarization control is required in fiber links.

Random polarization evolution also gives rise to polarization-dependent loss and polarization crosstalk. In links containing polarization-sensitive components such as polarizers, polarization beam splitters, waveguide couplers, and integrated modulators, the transmission, reflection, and coupling efficiencies are generally different for different polarization components. As a result, when the incident polarization state drifts, the output power, interference visibility, or modulation depth fluctuates accordingly, leading to polarization-dependent loss. If the two orthogonal polarization channels are not perfectly separated or if modal coupling exists, polarization crosstalk will occur, causing mutual mixing between nominally independent polarization signals and thereby reducing the extinction ratio, increasing the noise floor, and degrading sensing or communication performance. Therefore, the physical origin of polarization instability in fiber links can be understood through the chain of local birefringence variation, polarization-mode coupling, stochastic polarization evolution, and the subsequent emergence of polarization-dependent loss and polarization crosstalk.

2.2. Target parameters for polarization control

To evaluate the suitability of polarization-control techniques for different fiber-link applications, a multidimensional set of performance metrics is usually required. Among them, the polarization extinction ratio (PER) is one of the most important parameters, as it quantifies the separation capability between the target polarization state and its orthogonal counterpart. For strongly polarization-sensitive systems such as interferometric sensors and fiber-optic gyroscopes, a high PER generally implies lower polarization-induced noise and higher measurement accuracy [20]. Insertion loss reflects the influence of a polarization-control device on the link power budget. In long-distance transmission, weak-signal detection, and coherent reception, excessive additional loss directly reduces the dynamic range and signal-to-noise ratio of the system; therefore, low insertion loss remains an essential design objective.

For active polarization-control systems, response speed or switching time, locking time, and post-lock intensity fluctuation are key parameters for characterizing dynamic performance. Response speed or switching time determines the minimum time required for the device to complete polarization adjustment. Locking time describes the time required for a closed-loop system to converge from an initial disturbed state to the target polarization state. Post-lock intensity fluctuation directly reflects the stability and residual error of the locked state [21]. In rapidly varying environments or high-speed modulation links, a high static extinction ratio alone is insufficient; both fast tracking capability and stable locking performance are required to effectively suppress the degradation caused by dynamic polarization drift.

In addition, control accuracy, long-term stability, power consumption, and integration level/device footprint are also important performance indicators [22]. Control accuracy determines whether the polarization state can be stably maintained near the optimal operating point, whereas long-term stability reflects the ability of the system to preserve consistent performance under temperature drift, device aging, and environmental perturbations. For portable, arrayed, and on-chip systems, low power consumption, compact size, and high integration density are especially important because these factors affect engineering feasibility, packaging, thermal management, and multichannel scalability. Accordingly, the optimization target of modern polarization-control technologies has gradually shifted from pursuing a single high extinction ratio toward a more comprehensive balance of high extinction ratio, low loss, fast response, low power consumption, and high integration.

2.3. Application-specific requirements for polarization control

The priorities of polarization control vary across different application scenarios. For fiber-optic gyroscopes and interferometric fiber-optic sensing systems, polarization noise directly affects fringe visibility, bias stability, and measurement accuracy. In resonant or interferometric fiber-optic gyroscopes, random polarization coupling may introduce nonreciprocal phase errors and polarization-induced intensity fluctuations, which can degrade rotation-signal stability and increase bias drift. Accordingly, these systems generally require high-extinction-ratio polarization control, low polarization-coupling noise, and excellent long-term stability to maintain accurate and stable operation under environmental perturbations. Recent studies on fiber-optic gyroscopes have shown that improving the extinction ratio of resonators or polarization-selective components can effectively suppress polarization-induced noise and enhance bias stability, highlighting the importance of combining strong polarization selectivity with stable long-term operation in such systems.

For fiber-optic magnetic-field or current sensing, especially in sensing links based on polarization rotation or polarization analysis, the polarization state directly influences sensitivity and demodulation accuracy. Because a relatively long lead fiber is often present ahead of the sensing head, unknown polarization perturbations in the transmission fiber can change the polarization state incident on the sensitive element and thereby shift the system away from its optimal measurement point [23]. As a result, these applications typically require not only a high extinction ratio but also rapid and effective compensation of polarization distortion induced by the link. When the system is intended for dynamic measurement or online monitoring, the importance of polarization switching speed and real-time tracking capability becomes even more pronounced.

In coherent optical communication, polarization control mainly serves polarization multiplexing, polarization demultiplexing, and the stabilization of coherent reception. With the development of high-order modulation formats and high-speed coherent transmission, polarization drift may cause carrier fading, channel crosstalk, and increased digital-equalization complexity. Consequently, communication systems place greater emphasis on dynamic polarization-tracking speed, endless operation, and compatibility with digital signal processing [21, 24]. Recent research has identified high-speed polarization tracking and adaptive polarization control as key means of suppressing polarization fading in coherent systems, demonstrating that the requirements in communication scenarios are strongly oriented toward high speed, continuity, and automatic closed-loop operation [25].

By contrast, laboratory polarization adjustment and general optical bench setups usually place more weight on low loss, repeatability, and operational flexibility, while imposing relatively less stringent requirements on ultrafast switching or long-term automatic tracking. In such scenarios, polarization control is mainly used for initial polarization-state setting, experimental parameter scanning, or component characterization, and the goal is to achieve stable and repeatable adjustment in as simple a manner as possible. Overall, the target functions of polarization control differ substantially among applications: gyroscopes and interferometric sensors emphasize stability and extinction ratio, magnetic-field/current sensors emphasize high extinction ratio and rapid compensation, coherent communication emphasizes high-speed dynamic tracking and system compatibility, and laboratory adjustment emphasizes low loss and flexibility. These differences also imply that no single polarization-control solution can satisfy all application requirements simultaneously.

3. Passive Polarization Control in Fiber Links

Passive fiber polarization control was explored through loop-based architectures that combined PM fibers, special-angle splicing, and fiber polarization couplers/splitters to realize deterministic polarization routing in a reciprocal fiber path [26, 27]. The optical path was configured with two fiber polarization couplers/splitters and a PM fiber loop containing one 90° splice, such that the incident polarization state was transformed into its orthogonal counterpart after the first pass and then re-injected into the loop [28]. The schematic illustration of the principle is shown in Figure 2, where the incident polarization state is converted into its orthogonal counterpart through reciprocal propagation in the PM fiber loop. This design enabled two-pass propagation of polarized light in the sensing loop and achieved a twofold enhancement in angular-velocity sensitivity, while also providing compensation for transverse-strain-induced perturbations.

Figure 2
Schematic of passive fiber polarization control in a reciprocal fiber loop with two-pass polarization transformation

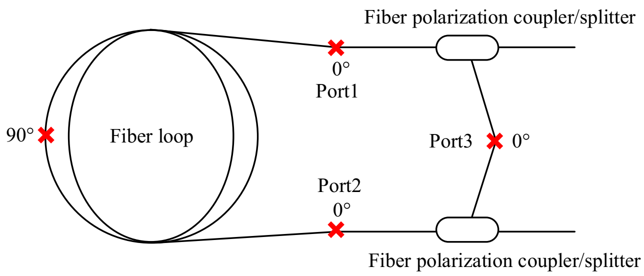

Subsequent efforts focused on reducing optical complexity without sacrificing the sensitivity enhancement factor. Zhou et al. [29] replaced two 1×2 fiber polarization couplers/splitters with a single 2×2 device, thereby reducing the number of discrete optical components and decreasing the optical path volume without sacrificing the twofold sensitivity enhancement. Wang et al. [30] further simplified the structure by introducing two 45° PM-fiber splices, which split the incident light into two orthogonal polarization components with equal intensity and eliminated the need for dedicated polarization couplers/splitters altogether. In this case, the key advantage was the further reduction of component count, whereas the main penalty was additional splice-induced insertion loss caused by the extra PM-fiber splice points. However, these early passive schemes all relied on a 90° splice inside the fiber loop, and the mechanical instability of this internal splice degraded loop robustness under rotational and vibrational conditions. To address this limitation, Zhang et al. [31] proposed a modified passive scheme in which the internal 90° splice was removed from the loop and transferred to the external control path by means of 0° splicing between the horizontal and vertical polarization output ports of two fiber polarization couplers/splitters. The optical path is shown in Figure 3 [31], in which the 90° splice is relocated outside the sensing loop to improve vibration tolerance and structural stability. Although the effective circulation number remained two passes, this design improved vibration tolerance and structural stability by eliminating the unstable splice point from the sensing loop itself.

Figure 3
Schematic of the counterclockwise optical path of the passive fiber polarization-control scheme with external splice-point relocation for improved structural stability

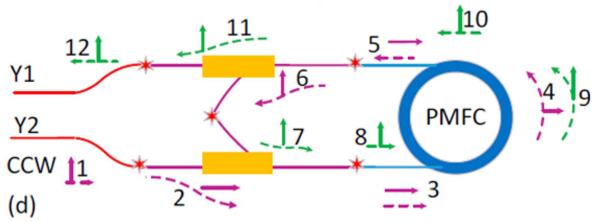

Recent researches have extended passive polarization control beyond loop-based fiber architectures and have highlighted several new performance-oriented directions. One direction is the use of all-PM fiber architectures, in which the principal technical indicators are no longer circulation number or switching speed, but rather polarization stability, repeatability, and resistance to environmental perturbations. In such systems, fixed birefringent axes and PM splicing reduce sensitivity to external disturbances and improve long-term operational consistency, making them attractive for applications that prioritize passive stability over reconfigurability [32].

Another direction is the incorporation of polarization-diversity passive structures into interferometric sensing systems, where the relevant metrics are suppression of polarization-induced fading, demodulation robustness, and noise reduction rather than dynamic tuning capability. A recent example is the integration of polarization diversity into a 3 × 3 coupler-based passive demodulation system for interferometric fiber-optic sensors, as shown in Figure 4 [33], where polarization diversity is introduced into the dual Sagnac interferometer to suppress polarization-induced fading and improve demodulation robustness [33]. In resonant fiber-optic gyroscopes, passive structures with enhanced polarization selectivity are increasingly evaluated by PER, polarization-noise suppression capability, and bias stability. Recent work has shown that high-extinction-ratio resonator designs can suppress polarization-induced noise and improve gyroscope stability [23]. A further trend is the development of compact passive or quasi-passive integrated photonic implementations, in which the dominant technical indicators become footprint reduction, integration density, structural stability, and multifunctional optical routing. Recent studies on integrated optical gyroscopes and thin-film lithium-niobate (TFLN) multifunctional photonic chips illustrate this direction toward compact and highly integrated photonic links [34, 35].

These studies show that passive polarization control still offers clear advantages in terms of low control overhead, compactness, reciprocity, and structural simplicity, but its intrinsic limitation remains unchanged, as the achievable polarization state and control function are fixed by design and cannot be adaptively updated in real time. This trade-off is consistently reflected across all-PM architectures, passive polarization-diversity demodulation systems, high-PER resonator schemes, and compact integrated passive implementations. Therefore, active polarization-control technologies are still required in dynamically perturbed fiber links and applications demanding real-time polarization tracking and adaptive compensation.

4. Active Polarization Control in Fiber Links

Active fiber polarization control achieves real-time regulation of the state of polarization by applying time-varying electric fields, magnetic fields, or mechanical stress to the optical path, thereby dynamically modifying the phase relationship or coupling state between orthogonal polarization components. According to the device type and underlying mechanism, existing active fiber polarization-control techniques can be broadly classified into fiber polarization controllers, Faraday-effect-based polarization-control technologies, and lithium-niobate electro-optic polarization-control technologies. Compared with passive polarization control, active techniques offer the advantages of real-time tunability, fast response, and strong adaptability to dynamic perturbations, but they also face challenges such as increased control complexity, higher power consumption, and

Figure 4
Schematic diagram of the dual Sagnac interferometer with polarization diversity for suppressing polarization-induced fading

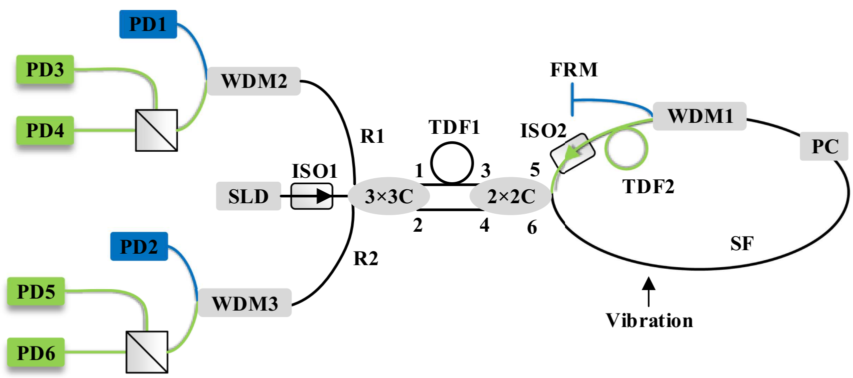

stricter system-stability requirements. Recent studies have shown that active polarization control is evolving from conventional discrete devices toward high-speed closed-loop control and integrated photonic platforms [36–40].

4.1. Manual fiber polarization controllers

Fiber loop waveplate polarization controllers generate controllable birefringence by winding the fiber into loops with specific radii, so that the bent fiber functions as an equivalent waveplate. Their operating principle is based on bending-induced birefringence, in which transverse stress and geometric deformation modify the refractive-index distribution in the fiber cross-section and create different propagation constants along two orthogonal polarization directions. By adjusting the angle between the bending plane and the incident polarization direction, the effective waveplate orientation can be controlled. In practice, two or three cascaded fiber loops are often used to form a polarization controller, and arbitrary polarization transformation can be achieved by adjusting the orientations of the equivalent quarter-wave and half-wave plates [41]. Fiber squeezer polarization controllers operate by applying transverse pressure to the fiber through piezoelectric actuators or mechanical squeezing blocks, thereby introducing controllable stress-induced birefringence and changing the phase difference between orthogonal polarization components [42]. Similar to loop-type controllers, their basic mechanism is also stress-induced birefringence, but squeezer-type devices are more amenable to electrical actuation and therefore have greater potential in automatic polarization-control systems. These devices usually exhibit low insertion loss, weak wavelength dependence, and relatively compact structures, and they have been widely used in quantum communication, coherent optics experiments, and automated mode-locked fiber-laser systems [43].

These devices are structurally simple, exhibit low insertion loss, and have relatively low cost, and they have long been widely used for initial polarization adjustment in laboratory optical systems, fiber sensing systems, and nonlinear polarization rotation fiber lasers [44–46]. Recent studies indicate that such loop-type polarization controllers are still frequently used in multi-wavelength or switchable fiber-laser systems, where they mainly serve for initial polarization optimization and operating-point setting rather than high-speed automatic polarization tracking [42]. In terms of applicability, this type of controller is particularly suitable for scenarios with low real-time requirements but strong demands for low loss and intuitive operation. Its main advantages include simple structure, broad wavelength adaptability, high optical-power tolerance, and the absence of complex driving electronics. Its major drawbacks are low control precision, manual operation, and slow response, which make it unsuitable for automatic polarization compensation in dynamically perturbed environments and far from capable of satisfying sub-100-ns polarization switching requirements.

4.2. Faraday-effect-based polarization-control technologies

4.2.1. Principle of Faraday rotation

The principle of the magneto-optic Faraday effect is shown in Figure 5. Faraday rotators operate on the basis of the magneto-optic Faraday effect. When an external magnetic field is applied parallel to the direction of light propagation, the left- and right-circular polarization components experience different refractive indices in the magneto-optic medium, causing the polarization plane of linearly polarized light to rotate. The rotation angle is approximately proportional to the magnetic flux density, the Verdet constant of the material, and the optical path length in the magneto-optic crystal. Therefore, polarization control can be achieved by adjusting the applied magnetic field [47]. Compared with mechanically induced birefringence devices, Faraday rotators are nonreciprocal and offer fast response and relatively high environmental stability, making them attractive for systems requiring rapid polarization modulation or magnetically induced control.

4.2.2. Permanent-magnet Faraday rotators

Permanent-magnet Faraday rotators employ fixed magnets as the magnetic-field source and therefore exhibit simple structure, compact size, and high stability, making them suitable for miniaturized and modular systems [48]. These devices can provide a predetermined fixed rotation angle and are useful in certain fiber sensing, isolation, and polarization pre-compensation applications. However, because the rotation angle is essentially fixed after fabrication, they cannot realize real-time control of arbitrary polarization angles, which limits their applicability in active polarization tracking. Recent studies have increasingly focused on high-Verdet-constant magneto-optic materials and compact integrated magneto-optic devices. For example, research on terbium-based magneto-optic ceramics and rare-earth iron garnet materials has shown that increasing the magneto-optic coefficient can significantly enhance the rotation efficiency per unit length, thereby shortening the required device length and reducing system size [49]. These material advances improve the engineering viability of permanent-magnet Faraday devices, although such devices still remain fundamentally limited by their fixed operating state.

4.2.3. Electromagnetically driven Faraday magneto-optic modulation

Electromagnetically driven Faraday magneto-optic modulators dynamically vary the magnetic field through current-driven coils, thereby enabling real-time tuning of the rotation angle of

Figure 5
Schematic of the magneto-optic Faraday effect

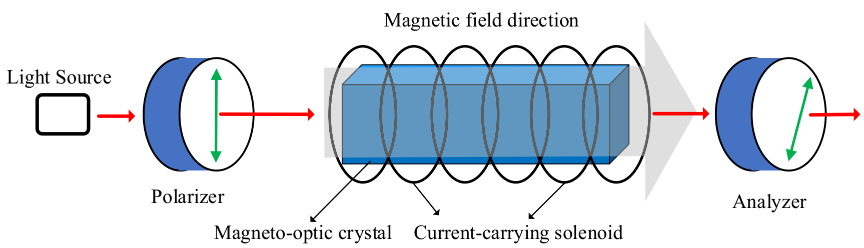

the magneto-optic crystal [50]. In principle, this approach allows real-time polarization control, and the Faraday effect itself can respond on the nanosecond scale. However, because the Verdet constants of commonly used magneto-optic materials are still limited, relatively strong magnetic fields are usually required when short crystal lengths are used. This increases coil size, power consumption, and thermal-management burden, which strongly constrains the application of this technology in compact fiber sensing systems, especially in probe-limited environments. Recent work suggests that the development of this route mainly depends on two directions: the exploration of magneto-optic materials with higher rotation efficiency and lower loss and the heterogeneous integration of magneto-optic garnets with silicon photonics and related platforms to reduce drive power and device size while preserving fast response [51]. Compared with electro-optic active polarization control, electromagnetically driven Faraday modulation remains less competitive in terms of programmability, power efficiency, and system integration, and it is therefore more often regarded as a complementary solution for specific magneto-optic sensing or polarization-modulation scenarios.

4.3. Lithium-niobate-electro-optic-based polarization-control technologies

4.3.1. Basic principle of lithium-niobate polarization control

Lithium-niobate polarization-control devices operate on the basis of the intrinsic birefringence of the crystal and its linear electro-optic effect. As shown in Figure 6, when a bias voltage is applied across the electrodes, the refractive indices corresponding to different polarization directions are modified, thereby changing the phase difference between orthogonal polarization components and enabling polarization-state regulation [52]. Lithium-niobate devices offer fast response, high driving precision, compact size, and good compatibility with photonic integration and therefore have long been regarded as one of the core technical routes for high-speed active polarization control. Their main challenge is that the half-wave voltage is sensitive to temperature and device-state variations, which leads to drift of the operating point and eventual loss of polarization-control functionality if uncompensated. Consequently, real-time monitoring and closed-loop stabilization of the bias voltage are essential for maintaining stable high-extinction-ratio output. In recent years, with the rapid development of TFLN, lithium-niobate-based polarization control has evolved from conventional bulk or diffused-waveguide devices toward high-speed on-chip integrated platforms. Since 2022, several studies have demonstrated that TFLN can support a series of key polarization-control functions, including arbitrary polarization generation, fast polarization measurement, polarization scrambling, and automatic polarization control, while simultaneously offering low drive voltage, low loss, and compact size. These advances provide a new device foundation for the high-speed and highly integrated development of active polarization control [53].

4.3.2. Representative implementations of active polarization control based on lithium niobate

As shown in Figure 7 [54], Noe et al. [54] reported a polarization-control scheme using a commercial polarization converter composed of multiple cascaded lithium-niobate waveguides, combined with a polarization beam splitter and a gradient-descent algorithm, to achieve real-time locking of the bias voltages. This system realized a locking time of 41 µs and an intensity fluctuation of 0.11%, demonstrating the feasibility of high-speed and high-extinction-ratio active polarization control. However, the need for multiple cascaded waveguides increased optical loss and structural complexity.

Figure 7
Schematic of polarization control based on an eight-stage cascaded lithium niobate integrated optical waveguide

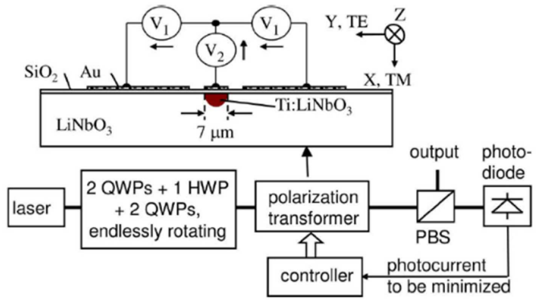

To reduce optical complexity, Mamdoohi et al. [55] proposed in 2012 an embedded polarization-control system based on a single lithium-niobate polarization controller and an optimized genetic algorithm, as shown in Figure 8(a). This approach reduced the number of active optical components but achieved a locking time of 300 µs and an intensity fluctuation of 6%, indicating that structural simplification came at the expense of dynamic performance. In 2013, Huang et al. [56] proposed a rapid positioning algorithm to overcome the poor convergence of

Figure 6
Schematic diagram of the principle of lithium-niobate polarization control

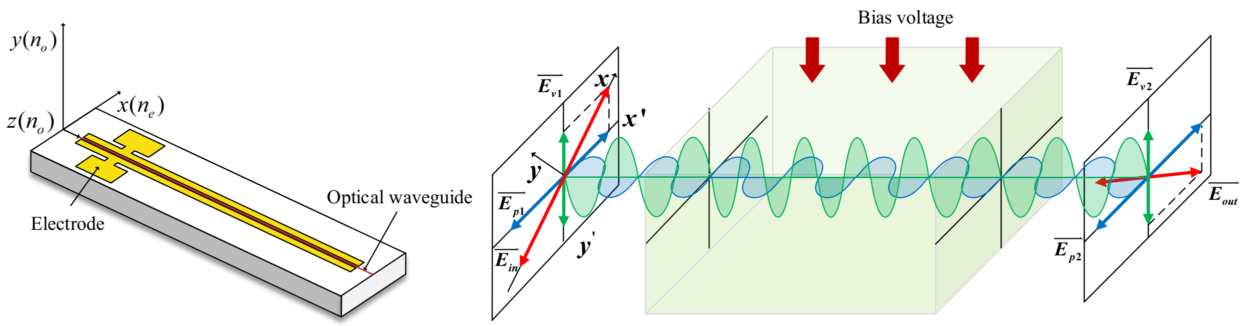

Figure 8
Representative schematic of a lithium-niobate-based active polarization-control scheme: (a) schematic of an embedded polarization-control system based on a genetic algorithm, (b) schematic of a high-bandwidth polarization-control technique based on an integrated photonic chip, (c) schematic of an integrated time-division polarization-control technique with high speed and high precision, and (d) the architecture and device dimensions of the adaptive polarization controller

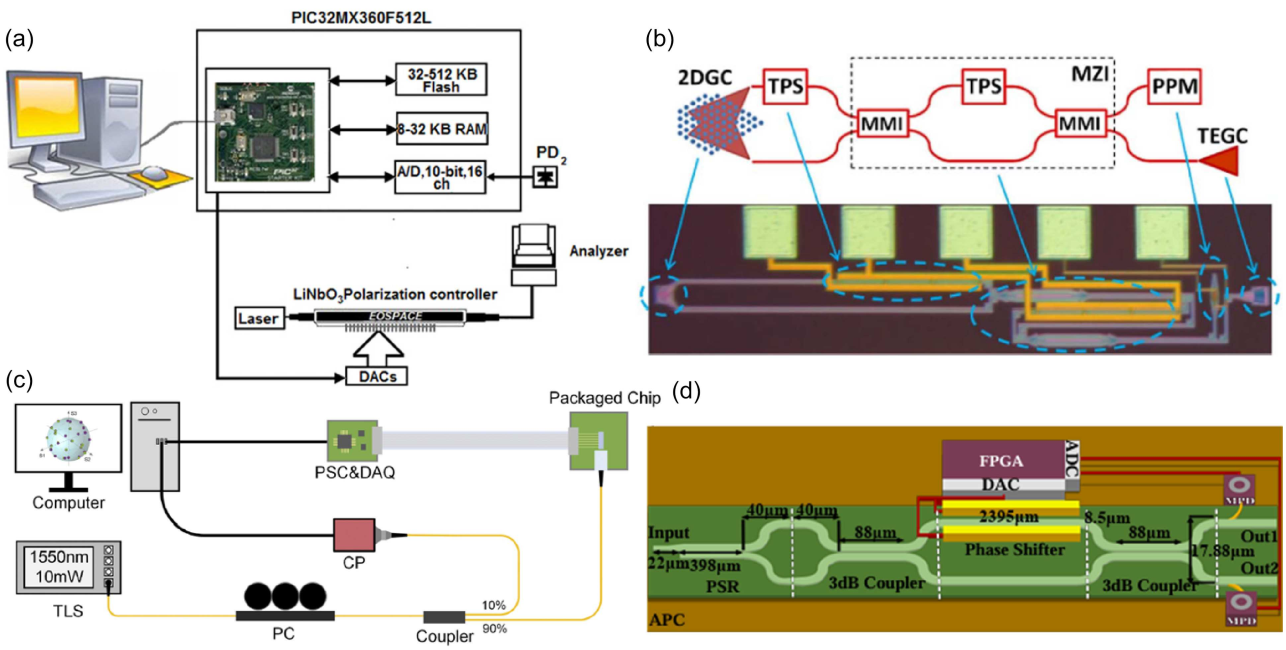

conventional simulated annealing and gradient-based methods, achieving intensity fluctuation below 1.5% after locking, although the locking time remained approximately 1 ms. These studies show that simultaneously reducing locking time and post-lock fluctuation without increasing optical complexity has long been a key challenge in active polarization control. In 2016, Velha et al. [57] proposed a high-bandwidth integrated polarization-control scheme based on photonic-chip structures composed of multimode interferometers, a Mach–Zehnder interferometer (MZI), and tunable polarizing splitters. As shown in Figure 8(b), this scheme achieved arbitrary polarization control, reduced the locking time to 10 μs, but increased the post-lock intensity fluctuation to 5%. In Figure 8(c), Liu et al. [58] reported a high-speed and high-precision time-division integrated polarization-control technique based on a balanced MZI, two photodetectors, and a combination of least-squares and singular-value-decomposition algorithms. The system achieved a locking time of 50 μs and an intensity fluctuation of 3%. These studies indicate that integration and algorithm optimization constitute the two main routes for improving the overall performance of active polarization control [59]. Li et al. [21] reported a high-speed polarization-tracking scheme based on an integrated TFLN dynamic polarization controller, in which a real-time Jacobian-based control algorithm was used to realize fast polarization tracking. Zhang et al. [60] proposed a variational mode decomposition (VMD)- and lock-in amplification (LIA)-based bias-control method for a lithium-niobate polarization controller. Their scheme compensated half-wave-voltage drift and stabilized the bias point, reducing the output intensity fluctuation from 3% to 0.017%, improving the signal-to-noise ratio by 398 times, achieving orthogonal polarization switching within 200 ns, and shortening the locking time to 15 μs. In 2024, Lin et al. [61] further proposed a lookup-table-based TFLN integrated polarization stabilizer, demonstrating the potential of TFLN for compact, low-power, and high-speed stable polarization control. Meanwhile, efforts to combine lithium niobate with other integrated platforms are continuing. As shown in Figure 8(d), simplified adaptive polarization controllers on lithium-niobate platforms were reported, using reduced structural complexity together with filtering algorithms to improve tracking performance and control efficiency [24]. In addition, for polarization-multiplexed communication, Tan et al. [25] demonstrated on-chip automatic polarization demultiplexing on a TFLN platform and achieved a maximum tracking speed of 600 rad/s in an 80 Gb/s polarization-multiplexed link while maintaining stable bit-error-rate performance under 100 rad/s perturbations. These results indicate that lithium-niobate-based active polarization control is moving beyond isolated polarization locking toward communication-grade high-speed applications. To facilitate a direct comparison of the representative active polarization-control schemes discussed above, Table 1 summarizes their key performance parameters, including platform type, locking time, intensity fluctuation, and insertion loss. The comparison shows that different schemes exhibit distinct trade-offs among response speed, locking stability, integration complexity, and optical loss.

4.4. Other active polarization controllers

In addition to mechanically induced [40–43], Faraday-effect-based [36, 48–51], and lithium-niobate-electro-optic polarization controllers [21, 52–61, 62], several other active polarization-control schemes based on emerging materials and platforms have been developed in recent years, mainly including silicon-photonic polarization controllers [63], liquid-crystal-integrated polarization controllers [64], and other heterogeneously integrated polarization-control devices [65]. These devices generally follow

Table 1
Comparison of the performance parameters of active polarization controllers

Refs.	Platform	Locking time (μs)	Intensity fluctuation	Insertion loss
[54]	Cascaded $LiNbO_3$ polarization waveguide controller	41	0.11%	Not reported
[55]	Genetic-algorithm-assisted single $LiNbO_3$ polarization controller	300	6%	Not reported
[56]	Fast-locating-algorithm-assisted four-plate polarization controller	1000	1.5%	Not reported
[57]	Silicon-photonic integrated polarization controller	10	5%	~3 dB
[58]	Integrated time-division polarization controller	50	3%	Not reported
[21]	TFLN integrated dynamic polarization controller	1.6	Not reported	$<$ 2 dB
[60]	Intelligent-algorithm-assisted $LiNbO_3$ polarization controller	15	0.017%	~3 dB

the same development trend of active polarization control toward high speed, programmability, and integration, while exhibiting different characteristics in terms of control mechanism, driving method, device size, and application scenarios [66, 67].

4.4.1. Silicon-photonic active polarization controllers

Active polarization controllers on silicon-photonic platforms usually rely on thermo-optic effects, carrier-dispersion effects, or phase-shifting structures, combined with polarization converters, MZIs, and phase-modulation units, to achieve on-chip polarization-state regulation and automatic tracking. Their major advantages lie in CMOS compatibility, relatively low fabrication cost, and suitability for large-scale integration, making them attractive for coherent communication, on-chip optical interconnects, and automatic polarization control. In 2024, a CMOS-compatible high-speed endless automatic polarization controller was reported, demonstrating silicon-based high-speed automatic polarization control through an innovative tuning structure and control strategy [10]. In the same year, another study proposed an ultra-compact on-chip silicon polarization controller that achieved a PER exceeding 54 dB over the wavelength range of 1530–1620 nm, highlighting the potential of silicon photonics for highly integrated and high-performance polarization control [68]. Furthermore, Juan Esteban Villegas et al. reported that inverse-designed ultra-compact polarization rotator-splitter structures combined with high-speed positive-type semiconductor and negative-type semiconductor (PN)-junction phase shifters could be used to construct high-bandwidth silicon-photonic polarization-control systems [69]. As shown in Figure 9 [69], the polarization rotator-splitter had a length of only 17 μm, an insertion loss below 1.0 dB across the C band and below 0.5 dB at 1550 nm, and an extinction ratio above 20 dB, indicating that silicon-photonic polarization controllers are evolving toward higher speed, lower loss, and more compact footprints.

Overall, the main advantages of silicon-photonic active polarization controllers include platform maturity, high integration density, compact device size, and compatibility with co-integration of detectors, modulators, and driving electronics. Their limitations lie in the relatively limited speed of thermo-optic tuning and the presence of thermal crosstalk, whereas carrier-based high-speed tuning often introduces additional loss and design complexity. Therefore, achieving a balance among speed, loss, power consumption, and integration density remains a key issue for the further development of silicon-photonic active polarization controllers.

4.4.2. Liquid-crystal-integrated active polarization controllers

Liquid-crystal materials have also been employed in emerging active polarization controllers because of their electrically tunable birefringence. Compared with lithium-niobate-based and silicon-photonic-based active polarization-control technologies, recent studies on liquid-crystal-integrated photonic platforms have been more focused on tunable photonics, programmable photonics, and reconfigurable waveguide devices rather than dedicated ultrafast polarization controllers. Consequently, current liquid-crystal-based polarization-control studies mainly emphasize low-power tunability, compact integration, and reconfigurable

Figure 9
Graphic representation of the high-speed polarization control in integrated silicon photonics

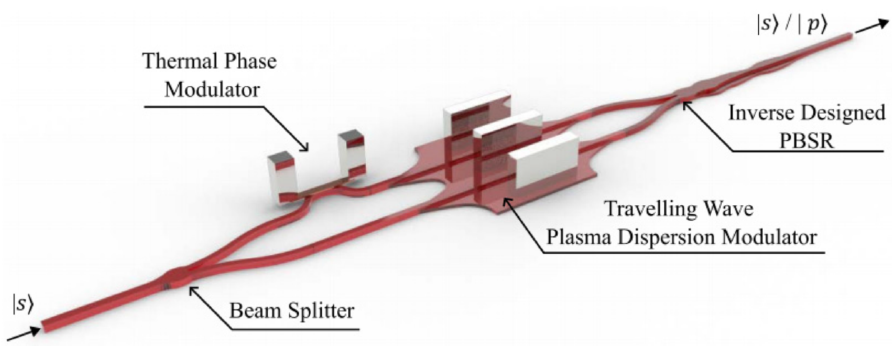

optical functionality instead of high-speed polarization-tracking performance.

Recent studies have further promoted the development of liquid-crystal-integrated polarization-control devices in integrated photonics. Lammers et al. [70] demonstrated electrically tunable polarization control in liquid-crystal-integrated femtosecond laser-written waveguides. As shown in Figure 10(a), electrically driven liquid-crystal reorientation was used to dynamically modify the birefringence and polarization response of the integrated waveguide structure [70]. The Pol. is a polarizer. The $\lambda/2$ is a half-wave plate. The device exhibited good tunability and compact integration capability, highlighting the potential of liquid-crystal-assisted photonic platforms for reconfigurable polarization manipulation. In Figure 10(b), Sharma and Sinha [71] developed a liquid-crystal channel-waveguide polarization selector based on electrically tunable birefringence. In Figure 10(b), P represents the polarizer, HWP represents the half-wave plate, MO represents the microscope objective, SMF represents the single-mode fiber, and LCW represents the liquid-crystal waveguide. The device achieved a Freedericksz transition voltage of approximately 1 V, an operating threshold of approximately 2 V, insertion loss of approximately 3.27 dB, and PERs exceeding 25 dB. More recently, Diao et al. [72] proposed an on-chip tunable polarization converter using liquid-crystal cladding in slab waveguides. The schematic of the chip is shown in Figure 10(c), where LS represents the laser source, L1 and L2 represent convex lenses, PL represents the polarizer, IC represents the camera, and Dt represents the detector. By electrically controlling the anisotropic dielectric tensor of the liquid crystal, dynamic Transverse Electric/Transverse Magnetic (TE/TM) mode conversion was achieved, with maximum PERs of 20.88 dB and 17.41 dB and ultralow power consumption of approximately 0.28 mW. Compared with lithium-niobate electro-optic polarization controllers, liquid-crystal-based devices generally exhibit lower driving voltage and lower power consumption, but their response speed and long-term environmental stability remain comparatively limited. Compared with silicon-photonic active polarization controllers, liquid-crystal-integrated devices provide stronger birefringence tunability and flexible reconfigurability, although they are currently less suitable for ultrafast polarization-tracking applications.

5. Summary

This review summarizes the recent progress in polarization control for fiber links and shows that passive schemes are simple and compact but inherently lack real-time adaptability, whereas active schemes offer higher speed, precision, and flexibility at the cost of greater complexity. In interferometric fiber-optic sensing systems such as fiber-optic gyroscopes, improved polarization-control performance can effectively suppress polarization-induced phase noise and bias drift, thereby enhancing rotation-sensing accuracy and long-term stability. In coherent optical communication systems employing polarization-division multiplexing, rapid and accurate polarization tracking can improve polarization demultiplexing performance, reduce signal distortion caused by polarization fluctuations, and enhance transmission reliability

Figure 10

Representative schematic of liquid-crystal-integrated active polarization controllers: (a) schematic of a femtosecond-laser-written waveguide using an embedded liquid-crystal cell, (b) experimental setup to characterize a low threshold electro-optic switch and TE/TM polarization selector, and (c) the experimental measurement of the on-chip tunable polarization converter

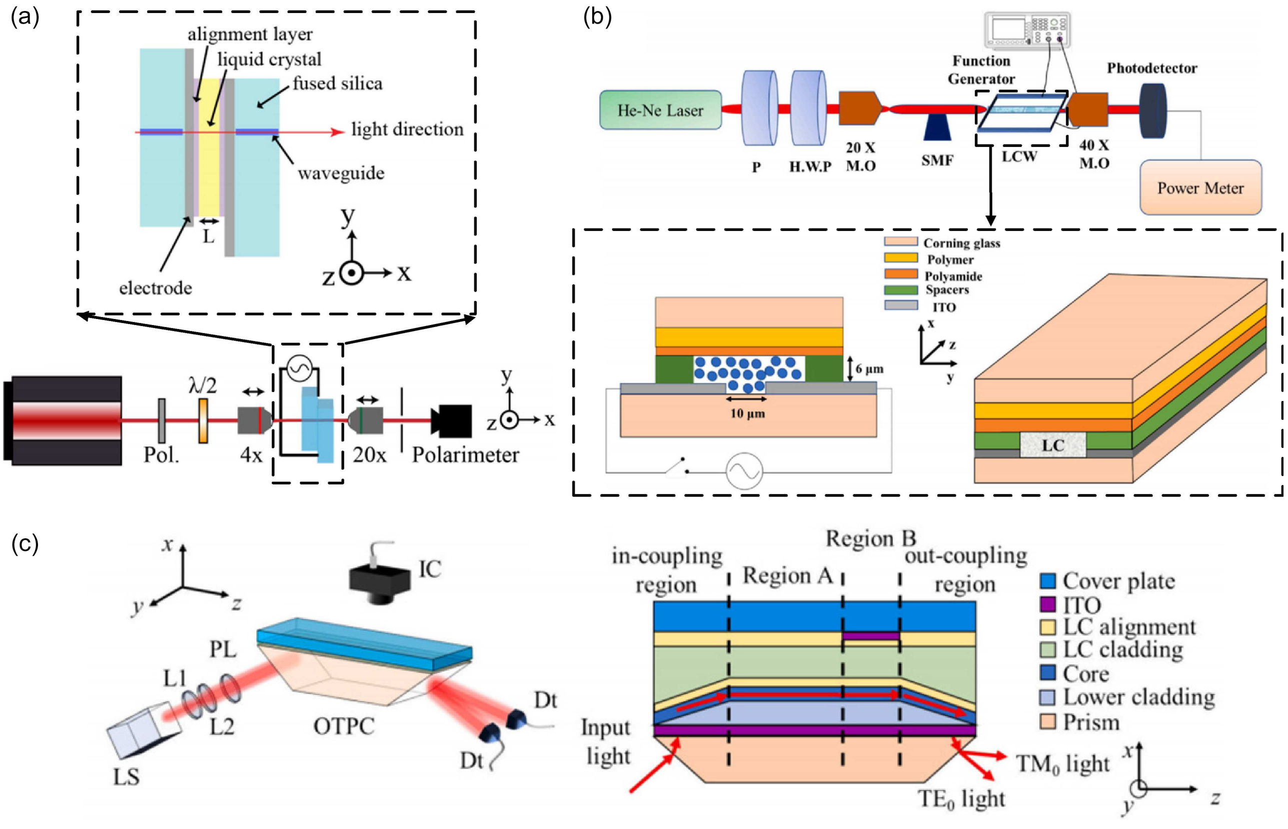

and spectral efficiency. Recent advances, especially in lithium niobate, silicon photonics, and integrated closed-loop control, have significantly improved the response speed, integration level, and control precision of active polarization control.

Despite these advances, achieving an effective balance among ultrafast response speed, high extinction ratio, low insertion loss, low power consumption, compact integration, and long-term environmental stability remains a critical challenge for next-generation polarization-control systems. Overall, future development is expected to continue toward faster response, higher integration density, lower power consumption, lower insertion loss, and better long-term stability through TFLN platforms, silicon photonics, heterogeneous integration, and intelligent closed-loop control strategies, thereby supporting next-generation high-performance fiber-optic sensing and high-capacity optical communication systems.

6. Recommendations

Future research on polarization control in fiber links should focus on achieving a better balance among response speed, extinction ratio, insertion loss, power consumption, integration level, and long-term stability. In particular, more attention should be given to the development of high-speed and low-power integrated polarization controllers based on TFLN, silicon photonics, and heterogeneous platforms, as well as to the joint optimization of device structures and closed-loop control algorithms. For interferometric fiber-optic sensing systems such as resonant fiber-optic gyroscopes, next-generation polarization-control technologies are expected to further suppress polarization-induced phase noise and bias drift, thereby improving rotation sensitivity and long-term measurement stability. In coherent optical communication systems employing polarization-division multiplexing, advanced polarization-control techniques can further enhance polarization demultiplexing accuracy, reduce polarization-related signal distortion, and improve transmission reliability and spectral efficiency under high-capacity and dynamically varying transmission conditions. In addition, application-oriented designs for fiber-optic sensing and optical communication systems should be further strengthened so that polarization-control techniques can better satisfy the practical requirements of compactness, robustness, and real-time adaptability.

Funding Support

The authors acknowledge support from the National Natural Science Foundation of China (62375237) and the Natural Science Foundation of Shanghai, China (24ZR1423800).

Ethical Statement

This study does not contain any studies with human or animal subjects performed by any of the authors.

Conflicts of Interest

The authors declare that they have no conflicts of interest to this work.

Data Availability Statement

Data sharing is not applicable to this article as no new data were created or analyzed in this study.

Author Contribution Statement

Zhihang Zhang: Conceptualization, Methodology, Software, Validation, Formal analysis, Investigation, Resources, Data curation, Writing – original draft, Writing – review & editing, Visualization, Supervision, Project administration, Funding acquisition. **Yujie Zheng:** Software, Writing – review & editing. **Xiao Wu:** Project administration. **Jianhua Yang:** Investigation. **Heming Wei:** Resources, Supervision. **Long Ma:** Data curation. **Xiaohu Liu:** Writing – original draft. **Dapeng Han:** Formal analysis, Funding acquisition. **Lijun Miao:** Investigation, Visualization. **Dengwei Zhang:** Software, Validation, Supervision, Project administration, Funding acquisition.

References

[1] He, H., Jiang, L., Pan, Y., Yi, A., Zou, X., Pan, W., . . . , & Yan, L. (2023). Integrated sensing and communication in an optical fibre. *Light: Science & Applications*, *12*(1), 25. https://doi.org/10.1038/s41377-022-01067-1

[2] Rodriguez-Ramirez, D. A., Martinez-Angulo, J. R., Filoteo-Razo, J. D., Elizondo-Leal, J. C., Diaz-Manriquez, A., Jauregui-Vazquez, D., . . . , & Saldivar-Alonso, V. P. (2025). Review of optical fiber sensors: Principles, classifications and applications in emerging technologies. *Photonics*, *13*(1), 40. https://doi.org/10.3390/photonics13010040

[3] Petrovich, M., Numkam Fokoua, E., Chen, Y., Sakr, H., Adamu, A. I., Hassan, R., . . . , & Poletti, F. (2025). Broadband optical fibre with an attenuation lower than 0.1 decibel per kilometre. *Nature Photonics*, *19*(11), 1203–1208. https://doi.org/10.1038/s41566-025-01747-5

[4] Hu, C., Luo, B., Pan, W., Yan, L., & Zou, X. (2023). Adaptive polarization control for a fiber system based on the optimized AdamSPGD algorithm. *Applied Optics*, *62*(33), 8798. https://doi.org/10.1364/AO.503759

[5] Dowling, E., Morris, M., Baumgartner, G., Roy, R., & Murphy, T. E. (2023). Non-local polarization alignment and control in fibers using feedback from correlated measurements of entangled photons. *Optics Express*, *31*(2), 2316–2329. https://doi.org/10.1364/OE.475465

[6] Wu, Z., Wu, Z., & Sun, A. (2024). Long distance distributed optical fiber vibration sensing and positioning technology based on loop transmission polarization detection. *Measurement*, *225*, 114029. https://doi.org/10.1016/j.measurement.2023.114029

[7] Shahwar, D., Yoon, H. H., Akkanen, S.-T., Li, D., Muntaha, S. T., Cherchi, M., . . . , & Sun, Z. (2024). Polarization management in silicon photonics. *npj Nanophotonics*, *1*(1), 35. https://doi.org/10.1038/s44310-024-00033-6

[8] Linale, N., Sansa, A., Grande, I. L., Castelvero, L., & Pruneri, V. (2026). Coexistence of classical and polarization-encoded QKD signals over deployed fiber. *Optics Express*, *34*(5), 7566–7580. https://doi.org/10.1364/OE.583877

[9] Wang, F., Wu, Y., Xu, X., Zhang, R., Luo, Q., Lu, H., . . . , & Wu, S. (2023). Preparation and properties of novel (Tb1−xCex)3Sc2Al3O12 magneto-optical transparent ceramics with different doping concentrations. *CrystEngComm*, *25*(21), 3171–3180. https://doi.org/10.1039/D3CE00233K

[10] Wang, W., Zhou, Z., Zeng, Y., Liu, J., Yao, G., Wu, H., . . . , & Tang, M. (2024). CMOS-compatible high-speed endless automatic polarization controller. *APL Photonics*, *9*(6), 066116. https://doi.org/10.1063/5.0198227

[11] Nikic, A., Li, W., St-Arnault, C., Bernal, S., Qiu, B., Berikaa, E., . . . , & Plant, D. V. (2025). A WDM capable SiP polarization compensator that isolates the carrier laser. *Journal of Lightwave Technology*, *43*(18), 8612–8621. https://doi.org/10.1109/JLT.2025.3588315
[12] Zhang, Z., Liang, C., Yang, J., Zhou, Y., Zhang, D., Huang, T., & Che, S. (2023). Sagnac magnetic field sensor based on sinusoidal modulation and empirical mode decomposition. *Journal of Lightwave Technology*, *41*(14), 4862–4867. https://doi.org/10.1109/JLT.2023.3244932
[13] Zhou, X., Yi, D., Chan, D. W. U., & Tsang, H. K. (2024). Silicon photonics for high-speed communications and photonic signal processing. *npj Nanophotonics*, *1*(1), 27. https://doi.org/10.1038/s44310-024-00024-7
[14] Menyuk, C. R. (2024). Solitons in birefringent optical fibers and polarization mode dispersion. *Optics Communications*, *550*, 129841. https://doi.org/10.1016/j.optcom.2023.129841
[15] Kwon, S., Ryu, J., Woo, T., Kim, J., & Lee, J. H. (2026). A detailed investigation into birefringence characteristics of a 20/400-μm polarization maintaining large mode area double clad fiber depending on material and geometric properties. *Journal of Lightwave Technology*, *44*(4), 1512–1521. https://doi.org/10.1109/JLT.2025.3641699
[16] Aitkulov, A., Cappelletti, M., Orsuti, D., Schenato, L., Hayashi, T., Santagiustina, M., . . . , & Palmieri, L. (2024). Distributed twist sensing with uncoupled multi-core fibers using polarization-sensitive reflectometry. *Journal of Lightwave Technology*, *42*(18), 6585–6591. https://doi.org/10.1109/JLT.2024.3404098
[17] Wang, L., Liao, M., Yu, F., Li, W., Xu, J., Hu, L., & Gao, W. (2023). Thermal sensitivity of birefringence in polarization-maintaining hollow-core photonic bandgap fibers. *Photonics*, *10*(2), 103. https://doi.org/10.3390/photonics10020103
[18] Zhang, Q., Zheng, Y., Zhu, Y., Tang, Q., Yu, Y., & Wang, L. (2024). Temperature and twist sensor based on the sagnac interferometer with long-period grating in polarization-maintaining fiber. *Sensors*, *24*(2), 377. https://doi.org/10.3390/s24020377
[19] Yan, W., Wu, B., Jiang, X., Huang, Y., Wen, F., & Qiu, K. (2024). Polarization-dependent loss measurement on mode division multiplexing system for optimal transmission of high-speed dual-polarization signals. *Optics & Laser Technology*, *174*, 110627. https://doi.org/10.1016/j.optlastec.2024.110627
[20] Chen, L., Mao, Y., He, P., Wang, H., Jiang, B., & Zhao, J. (2023). Compact and high-reliability fiber-optic open-loop gyroscope enabled by an in-fiber polarizer. *Optics Express*, *31*(3), 4803–4811. https://doi.org/10.1364/OE.480935
[21] Li, Z., Gan, R., Xu, Y., Chen, B., Zhou, X., Liu, J., . . . , & Guo, C. (2023). High-speed polarization tracking using thin film lithium niobate integrated dynamic polarization controller. *Optics Express*, *31*(24), 39369–39378. https://doi.org/10.1364/OE.502187
[22] Miao, W., Zhao, H., Yu, F., & Li, L. (2025). A high-extinction-ratio resonator for suppressing polarization noise in hollow-core photonic-crystal fiber optic gyro. *Photonics*, *12*(11), 1126. https://doi.org/10.3390/photonics12111126
[23] Gusarov, A., Beaumont, P., & Siren, P. (2024). Performance enhancement of the polarimetric fibre optical current sensor at JET using polarisation optimisation. *Sensors*, *24*(2), 555. https://doi.org/10.3390/s24020555
[24] Liu, P., Ji, W., Wang, Y., Yin, X., Tan, X., & Wang, Z. (2025). Simplified adaptive polarization controller controlled by an alpha-beta filter for the self-coherent communication system. *Optics Express*, *33*(1), 788. https://doi.org/10.1364/OE.543935
[25] Tan, H., Lin, Y., Zhang, J., Wang, J., Ke, W., Lin, Z., & Cai, X. (2024). Polarization division multiplexing link using a high-speed lithium niobate automatic polarization demultiplexer. *Optics Letters*, *49*(23), 6593–6596. https://doi.org/10.1364/OL.533035
[26] Liu, Y., Lin, W., Zhao, F., Hu, J., Chen, J., Liu, H., . . . , & Shao, L. Y. (2023). Adaptive fiber ring laser based on tapered polarization maintaining fiber in Sagnac loop for temperature and salinity sensing. *Photonics*, *10*(5), 599. https://doi.org/10.3390/photonics10050599
[27] Ye, G., Chow, K. K., Liu, B., Dai, M., Ma, Y., Shirahata, T., . . . , & Set, S. Y. (2023). L-band mode-locked fiber laser using all polarization-maintaining nonlinear polarization rotation. *Optics Letters*, *48*(18), 4729–4732. https://doi.org/10.1364/OL.498865
[28] Li, C., Zhang, C., Song, N., & Xu, H. (2011). Polarization-maintaining fiber loop with double optical length and its application to fiber optic gyroscope. *Chinese Optics Letters*, *9*(2), 020604. https://doi.org/10.3788/COL201109.020604
[29] Zhou, K., Pan, S., Liu, S., & Hu, K. (2013). Fiber gyroscope with a double sensitivity employing a polarization splitter. *Optics Letters*, *38*(8), 1337–1339. https://doi.org/10.1364/OL.38.001337
[30] Wang, Z., Yang, Y., Lu, P., Luo, R., Li, Y., Zhao, D., . . . , & Li, Z. (2014). Dual-polarization interferometric fiber-optic gyroscope with an ultra-simple configuration. *Optics Letters*, *39*(8), 2463–2466. https://doi.org/10.1364/OL.39.002463
[31] Zhang, D., Liang, C., & Li, N. (2020). A novel approach to double the sensitivity of polarization maintaining interferometric fiber optic gyroscope. *Sensors*, *20*(13), 3762. https://doi.org/10.3390/s20133762
[32] Wang, Y., & Wang, M. (2025). Research progress on all-polarization-maintaining mode-locked fiber lasers. *Photonics*, *12*(4), 366. https://doi.org/10.3390/photonics12040366
[33] Hu, H., Wang, Q., Lai, X., Du, Z., Wu, H., Xiao, Q., & Jia, B. (2025). Integrating polarization diversity into 3 × 3 coupler passive demodulation for interferometric fiber-optic sensors. *Optics Express*, *33*(7), 16468–16482. https://doi.org/10.1364/OE.550507
[34] Ai, Q., Tan, M., Herbold, M., Russell, R., Dubey, A., Ren, G., . . . , & Mitchell, A. (2025). Integrated photonic gyroscopes. *Electromagnetic Science*, *3*(2), 0100261. https://doi.org/10.23919/emsci.2024.0026
[35] Wei, C., Feng, H., Ye, K., Eijkel, M., Klaver, Y., Chen, Z., . . . , & Marpaung, D. (2025). Programmable multifunctional integrated microwave photonic circuit on thin-film lithium niobate. *Nature Communications*, *16*(1), 2281. https://doi.org/10.1038/s41467-025-57441-1
[36] Mihailovic, P., & Petricevic, S. (2021). Fiber optic sensors based on the Faraday effect. *Sensors*, *21*(19), 6564. https://doi.org/10.3390/s21196564
[37] Lai, K., Yu, Y., Sui, Q., Wang, D., & Li, Z. (2023). Jacobian methods for dynamic polarization control in optical applications. *Optics Express*, *31*(8), 12175–12188. https://doi.org/10.1364/OE.486761
[38] Farsi, M., Häger, C., Karlsson, M., & Agrell, E. (2022). Polarization tracking in the presence of PDL and fast temporal drift. *Journal of Lightwave Technology*, *40*(19), 6408–6416. https://doi.org/10.1109/JLT.2022.3194734

[39] Wang, X., Jia, Y., Guo, X., Liu, J., Wang, S., Liu, W., . . . , & Li, Y. (2022). Silicon photonics integrated dynamic polarization controller. *Chinese Optics Letters*, *20*(4), 041301. https://doi.org/10.3788/COL202220.041301

[40] Braband, N., Mansouri, A., Fazili, R., Czischek, S., & Lundeen, J. S. (2025). Fast and automated optical polarization compensation of fiber unitaries. *Review of Scientific Instruments*, *96*(6), 063101. https://doi.org/10.1063/5.0249996

[41] Huang, Y., & Xia, R. (2023). Mueller matrix analysis of spun wave plate for arbitrary SOP conversion. *Optics Express*, *31*(22), 37250–37261. https://doi.org/10.1364/OE.497473

[42] Shi, Y., Qi, Y., Shen, H., Quan, Z., & Tang, M. (2024). Theoretical analysis on active polarization control of fiber laser based on root mean square propagation algorithm. *Applied Sciences*, *14*(21), 9691. https://doi.org/10.3390/app14219691

[43] Liu, X., Ye, F., Zhao, M., Malomed, B. A., Fu, H. Y., & Li, Q. (2023). All-polarization-maintaining linear cavity fiber lasers mode-locked by nonlinear polarization evolution in stretched pulse regime. *Journal of Lightwave Technology*, *41*(15), 5107–5115. https://doi.org/10.1109/JLT.2023.3250224

[44] Chen, B., Bracken, J., Verleyen, F., Wang, Y., & Xu, C. (2005). Analysis of all-optical intra-cavity wavelength conversions in fiber ring resonators. *Optics Communications*, *247*(1-3), 57–64. https://doi.org/10.1016/j.optcom.2004.11.048

[45] Zhu, Y., Ou, Y., Cheng, C., Xiao, W., Xie, Z., He, J., . . . , & Liu, W. (2023). Amplified frequency-shifted fiber loop ringdown pressure sensing. *Optics Communications*, *534*, 129327. https://doi.org/10.1016/j.optcom.2023.129327

[46] Cheng, J. (2022). Eight-wavelength EDF laser combining tilted fiber grating with sampled fiber grating. *Optics & Laser Technology*, *148*, 107730. https://doi.org/10.1016/j.optlastec.2021.107730

[47] Zhang, L., Hu, D., Snetkov, I. L., Balabanov, S., Palashov, O., & Li, J. (2023). A review on magneto-optical ceramics for Faraday isolators. *Journal of Advanced Ceramics*, *12*(5), 873–915. https://doi.org/10.26599/JAC.2023.9220742

[48] Li, L., Ma, Q., Cao, M., Zhang, G., Zhang, Y., Jiang, L., . . . , & Li, W. (2016). High stability Michelson refractometer based on an in-fiber interferometer followed with a Faraday rotator mirror. *Sensors and Actuators B: Chemical*, *234*, 674–679. https://doi.org/10.1016/j.snb.2016.05.045

[49] Yu, C., Ma, S., Ren, H., Chen, Z., Xiang, C., Yan, Y., . . . , & Zhou, T. (2022). AC field modulated DC magnetic field sensor based on optical whispering gallery mode microcapillary resonator. *Optics Express*, *30*(13), 24062–24071. https://doi.org/10.1364/OE.459338

[50] Ikesue, A., Aung, Y. L., & Wang, J. (2022). Progress of magneto-optical ceramics. *Progress in Quantum Electronics*, *86*, 100416. https://doi.org/10.1016/j.pquantelec.2022.100416

[51] Zhao, Y., Lv, R.-Q., Wang, D., & Wang, Q. (2014). Fiber optic Fabry-Perot magnetic field sensor with temperature compensation using a fiber Bragg grating. *IEEE Transactions on Instrumentation and Measurement*, *63*(9), 2210–2214. https://doi.org/10.1109/TIM.2014.2308360

[52] Lin, Z., Lin, Y., Li, H., Xu, M., He, M., Ke, W., . . . , & Cai, X. (2022). High-performance polarization management devices based on thin-film lithium niobate. *Light: Science & Applications*, *11*(1), 93. https://doi.org/10.1038/s41377-022-00779-8

[53] Wang, M., Yao, H., Deng, J., Hu, Z., Tang, T., & Chen, K. (2024). Polarization splitter-rotator on thin film lithium niobate based on multimode interference. *Optics Express*, *32*(16), 28175–28182. https://doi.org/10.1364/OE.530883

[54] Noe, R., Koch, B., Mirvoda, V., Hidayat, A., & Sandel, D. (2009). 38-krad/s 3.8-Grad broadband endless optical polarization tracking using $LiNbO_3$ device. *IEEE Photonics Technology Letters*, *21*(17), 1220–1222. https://doi.org/10.1109/LPT.2009.2024549

[55] Mamdoohi, G., Fauzi Abas, A., Samsudin, A., Ibrahim, N. H., Hidayat, A., & Mahdi, M. A. (2012). Implementation of genetic algorithm in an embedded microcontroller-based polarization control system. *Engineering Applications of Artificial Intelligence*, *25*(4), 869–873. https://doi.org/10.1016/j.engappai.2012.01.018

[56] Huang, Z., Liu, C., Li, J., Zhang, D., Cheng, H., Luo, Y., . . . , & Han, M. (2013). Fiber polarization control based on a fast locating algorithm. *Applied Optics*, *52*(27), 6663–6668. https://doi.org/10.1364/AO.52.006663

[57] Velha, P., Sorianello, V., Preite, M. V., de Angelis, G., Cassese, T., Bianchi, A., . . . , & Romagnoli, M. (2016). Wide-band polarization controller for Si photonic integrated circuits. *Optics Letters*, *41*(24), 5656–5659. https://doi.org/10.1364/OL.41.005656

[58] Liu, W., Liao, J., Yu, Y., & Zhang, X. (2021). High-efficient and high-accurate integrated division-of-time polarimeter. *APL Photonics*, *6*(7), 071302. https://doi.org/10.1063/5.0057625

[59] He, M., Xu, M., Ren, Y., Jian, J., Ruan, Z., Xu, Y., . . . , & Cai, X. (2019). High-performance hybrid silicon and lithium niobate Mach–Zehnder modulators for 100 Gbit s^{-1} and beyond. *Nature Photonics*, *13*(5), 359–364. https://doi.org/10.1038/s41566-019-0378-6

[60] Zhang, Z., Zhang, D., Liang, C., Yang, J., Che, S., & Shu, X. (2023). Bias control approach based on VMD and LIA demodulation of a lithium niobate polarization controller. *Applied Optics*, *62*(25), 6571–6576. https://doi.org/10.1364/AO.500485

[61] Lin, Y., Ke, W., Zhu, Y., Tan, H., Wang, J., Lin, Z., & Cai, X. (2024). High-speed thin-film lithium niobate integrated polarization stabilizer assisted by on-chip polarization analyzing. *Optics Express*, *32*(27), 48267–48275. https://doi.org/10.1364/OE.545614

[62] Wang, C., Zhang, M., Stern, B., Lipson, M., & Lončar, M. (2018). Nanophotonic lithium niobate electro-optic modulators. *Optics Express*, *26*(2), 1547–1555. https://doi.org/10.1364/OE.26.001547

[63] Liu, Q., Bian, Y., & Xiong, J. (2025). Progress in passive silicon photonic devices: A review. *Photonics*, *12*(9), 928. https://doi.org/10.3390/photonics12090928

[64] Xu, J., Yang, R., Fan, Y., Fu, Q., & Zhang, F. (2021). A review of tunable electromagnetic metamaterials with anisotropic liquid crystals. *Frontiers in Physics*, *9*, 633104. https://doi.org/10.3389/fphy.2021.633104

[65] Han, H., Ruan, S., & Xiang, B. (2025). Heterogeneously integrated photonics based on thin film lithium niobate platform. *Laser & Photonics Reviews*, *19*(1), 2400649. https://doi.org/10.1002/lpor.202400649

[66] Zafar, H., & Pereira, M. F. (2024). Recent progress in light polarization control schemes for silicon integrated photonics. *Laser & Photonics Reviews*, *18*(11), 2301025. https://doi.org/10.1002/lpor.202301025

[67] Pérez-López, D., & Torrijos-Morán, L. (2025). Large-scale photonic processors and their applications. *npj Nanophotonics*, *2*(1), 32. https://doi.org/10.1038/s44310-025-00075-4
[68] Zhao, W., Peng, Y., Zhu, M., Liu, R., Hu, X., Shi, Y., & Dai, D. (2024). Ultracompact silicon on-chip polarization controller. *Photonics Research*, *12*(2), 183. https://doi.org/10.1364/PRJ.499801
[69] Villegas, J. E., Tamalampudi, S. R., & Rasras, M. (2025). High-speed polarization control in integrated silicon photonics. *Optics Express*, *33*(8), 18477. https://doi.org/10.1364/OE.523366
[70] Lammers, K., Alberucci, A., Jisha, C. P., Szameit, A., & Nolte, S. (2024). Electro-optical control of polarization in femtosecond-laser written waveguides using an embedded liquid crystal cell. *Optical Materials Express*, *14*(4), 836–846. https://doi.org/10.1364/OME.507230
[71] Sharma, V., & Sinha, A. (2023). Low threshold electro-optic switch and TE/TM polarization selector using liquid crystal channel waveguide. *Optics & Laser Technology*, *159*, 108987. https://doi.org/10.1016/j.optlastec.2022.108987
[72] Diao, Z., Fan, W., Yu, Y., Bi, Z., Zhao, H., Wang, Y., . . . , & Mu, Q. (2025). On-chip tunable polarization converter for slab waveguide based on liquid crystal. *Optics & Laser Technology*, *192*, 114148. https://doi.org/10.1016/j.optlastec.2025.114148

How to Cite: Zhang, Z., Zheng, Y., Wu, X., Yang, J., Wei, H., Ma, L., …, & Zhang, D. (2026). Recent Advances in Polarization Control for Fiber Links: Mechanisms, Technologies, and Applications. *Journal of Optics and Photonics Research*. https://doi.org/10.47852/bonviewJOPR62029745